The impact of oxygen heterogeneity on epithelial-mesenchymal transitions: a numerical study

Gopinath Sadhu[a,*], Helen M. Byrne[b,c], D. C. Dalal[a]

[a] *Department of Mathematics, Indian Institute of Technology Guwahati, Assam, India*
[b] *Wolfson Centre for Mathematical Biology, Mathematical Institute, University of Oxford, Oxford, United Kingdom*
[c] *Ludwig Institute for Cancer Research, University of Oxford, Oxford, United Kingdom*

Abstract

The epithelial-mesenchymal transition (EMT) is a key stage in tumor metastasis and invasion which transition depends on many micro-environmental factors, including oxygen levels. In this article, we use a continuum partial differential equations (PDEs) framework comprising coupled equations for the epithelial, mesenchymal, and necrotic cell densities and oxygen concentration to unravel the mysteries of how oxygen heterogeneity affects EMT. A distinguishing feature of the model is that the rates of EMT and MET (mesenchymal-epithelial transition) depend on the oxygen concentration. We assume EMT occurs when oxygen concentration drops below a critical level, and MET occurs when it rises above the critical value.

We begin by studying EMT dynamics in an *in vitro* scenario, where oxygen levels are assumed to be spatially uniform and fluctuate over time between normoxia and hypoxia. This setup mimics aspects of the *in vivo* phenomenon of cyclic hypoxia. Numerical simulations indicate that the tumor cells adopt a single phenotype based on the oxygen levels: under normoxic conditions, the cells exhibit an epithelial phenotype, while under hypoxic conditions, they transition to a mesenchymal phenotype. We also observe that temporal changes in oxygen levels affect the tumor's overall growth rate. Specifically, our investigations reveal that as the timescale of the oxygen fluctuations decreases, the tumor's growth rate increases.

We then use the model to study an *in vivo* scenario in which we account for oxygen diffusion in order to investigate the effect of spatial heterogeneity in oxygen levels on the EMT dynamics. Simulation results indicate that spatial oxygen heterogeneity generates a heterogeneous population within the tumor, with epithelial cells localized on the outer rim of the tumor and mesenchymal cells concentrated at the tumor center. We perform additional simulations which show further that an increase in mesenchymal diffusivity increases the density of the epithelial cells and the tumor's volume.

Keywords: Oxygen heterogeneity, epithelial to mesenchymal transition, mesenchymal to epithelial, tumor growth, cyclic hypoxia

*Corresponding author
Email address: gsadhu@iitg.ac.in (Gopinath Sadhu)

1. Introduction

The epithelial-mesenchymal transition (EMT) is a cellular process that occurs when epithelial cells achieve mesenchymal characteristics. EMT is a crucial event for various biological processes, including embryogenesis, wound healing, and cancer [1]. Epithelial tissue is well structured in cobblestone patterns with the help of cell-cell adhesive properties and a complex, tight chemical gene regulatory system. This epithelial phenotype is maintained by E-cadherin, which helps to stick epithelial cells together [2]. During EMT, cells lose their epithelial trait and adopt the spindle-shaped mesenchymal trait, helping to acquire an invasive phenotype [3].

In the context of cancer, EMT of tumor cells is the first move to achieve tumor migration and leads to destructive metastasis for cancer-related death. There are two main key features that are commonly manifested in the EMT process. First, the loss of proteins that characterize an epithelial phenotype, along with the acquisition of mesenchymal proteins, is regarded as the foundation of EMT [4]. Second, signals from the tumor microenvironment (TME) drive downregulation of epithelial genes and upregulation of mesenchymal genes by EMT-relevant transcription factors (e.g., SNAIL, SLUG, TWIST), leading to reorganization of the cell cytoskeleton [5]. These signatures have been described for many different types of carcinomas, such as lung, liver, breast, prostate, colorectal, head and neck, and ovarian. Scientific communities are hunting the cause of EMT in tumors. Many publications indicate that some defective genetic regulation is the reason behind EMT [6, 7, 8, 9]. Katz et al. [10] identified a 9-gene signature characteristic of EMT in breast cancer. They showed that these signatures demonstrate the hallmark of EMT, including loss of the E-cadherin protein and acquisition of the expression of N-cadherin and vimentin. Various investigations reveal that the EMT process can be reversible by silencing the signaling pathway involved in EMT. It is known as the mesenchymal-epithelial transition (MET) process. The processes EMT and MET are not binary. To complete EMT, epithelial cells first transit into hybrid epithelial/mesenchymal states and then switch to mesenchymal cells. The number of these hybrid states may be more than one in some tumors. However, under which circumstances this genetic malfunction is triggered in order to initiate the EMT or MET processes, these phenomena are not fully understood.

A well-established characteristic of the solid tumor is hypoxia [11]. Depending on the oxygen supply from the primary blood vessel near the tumor, a hypoxic region is found even in a tiny tumor. The oxygen gradient develops inside the tumor, which leads to oxygen heterogeneity in tumors. This variation in oxygen levels triggers several biological events, such as metabolic adaptation, angiogenesis, immunomodulation, and many more. Hypoxia is also a purported driver of EMT in tumors [12, 13]. In the hypoxic region, hypoxia-inducible factors (e.g., HIF-1α) are secreted by tumor cells. It has been proved that HIF-1α is the major mediator of hypoxia-driven EMT [14]. Zhang et al. [15] experimentally have shown that hypoxia stabilized HIF-1α promoted EMT by increasing SNAI1 transcription. The hypoxic tumor alters its metabolic process from oxidative phosphorylation to anaerobic glycolysis [16]. During the glycolysis process, hypoxic tumor cells secrete lactate and acidify TME [17]. Meanwhile, the secretion of lactate from cells elevates the intracellular pH, which activates Wnt signaling, potentially leading to EMT in order to help the metastasis cascade [18]. As hypoxia depends on the oxygen level within the tumor, a correlation exists between the oxygen levels in the tumor and the EMT process. Many experimental studies are devoted to decoding the mysteries of the interplay between oxygen levels and EMT dynamics. Depending on the oxygen level, epithelial cells acquire the mesenchymal phe-

notype and vice versa. However, how oxygen heterogeneity inside the tumor impacts the EMT dynamics and tumor growth remains to be studied. In addition, experimental work indicates that when epithelial tumor cells convert to the mesenchymal type, the mesenchymal cells develop aggressive motile characteristics. The effects of mesenchymal cell motility on EMT dynamics have not been explored. In *in vivo* tumor, cyclic hypoxia is a well-established characteristic in solid tumors. This characteristic can be closely mimicked by the precious control of oxygen supply to the tumor culture medium. The intricate relationship between cyclic hypoxia and EMT is not yet fully understood, and further research is required to uncover the underlying mechanisms and their potential implications for tumor growth dynamics.

The mathematical modeling framework offers an alternative approach for studying complex, time-consuming biological phenomena [19]. Mathematical models are classified into three categories; continuum, discrete, and hybrid models. Discrete modelings are employed to illustrate the individual basis interaction between cells and tumor micro-environmental species. Currently, there are several types of discrete modeling strategies available to describe cell populations, e.g., the cellular pot model, the agent-based model, and the cellular automata models [20]. Whereas in continuum modeling, cell populations and metabolic elements are treated as continuum species. Here, continuum species are modeled using ordinary differential equations (ODEs) and partial differential equations (PDEs). Lastly, in hybrid modeling, both continuous and discrete modeling approaches are adopted. Many authors demonstrate the EMT process through a system of ODEs using the compartmental model [21, 22, 23]. In EMT program, a large number of EMT transcription factors are involved. He et al. [24] proposed a minimal dynamical model to investigate EMT and MET processes of tumor cells based on the transcriptional regulatory mechanisms between microRNA-200 and ZEB transcription factors in an individual tumor cell. Recently, Tripathi et al. [25] explored the mechanism for epithelial-mesenchymal heterogeneity in a population of cancer cells using ODE-based mathematical modeling. Their study highlights how factors known to promote a hybrid epithelial-mesenchymal phenotype can alter the phenotypic composition of a population. EMT and MET processes are not readily captured with an ODE-based model, as these processes interlink with spatial interactions with the tumor surrounding medium, nutrient gradients, and oxygen heterogeneity.

Several PDE models have been developed to describe tumor growth and invasion [26, 27, 28, 29, 30]. For example, Chaplain and Lolas [31] proposed a model to study the impact of urokinase-type plasminogen activator and matrix metalloproteinases on cancer invasion. Recent experimental results highlight that during tumor progression, tumor cells adopt the go-or-grow hypothesis [32]. Recently, Crossley et al. [29] used a phenotypic switching framework based on the go-or-grow hypothesis to study tumour invasion. The classification of phenotypic characteristics is not limited to the go-or-grow hypothesis. Prasanna et al. [33] classified tumor cell populations as epithelial or mesenchymal according to their cell-cell and cell-ECM adhesion strengths. They used a cell-based model to investigate how spatial heterogeneity in cell-cell and cell-ECM adhesion influences tumor invasiveness. EMT and invasion cascades are influenced by multiple environmental factors, including hypoxia, lactate and multiple growth factors [34, 35]. Sfakianakis et al.[36] used a multiscale framework to study the effects of epidermal growth factors (EGFs) on EMT dynamics. Hypoxia is a hallmark of cancer progression, and has a significant effect on both tumor cell proliferation and metastasis [13, 11]. Numerous mathematical models have been proposed to elucidate its roles on solid tumor growth, necrotic core evolution, angiogenesis, and metabolic adaptation [37, 38, 39, 40]. In 1972, a seminal work by Greenspan [40] presented a mathematical model in

which tumor growth is limited by the diffusion of nutrients. This approach has been adopted by many other authors to study the effects of hypoxia and the microenvironment on tumor progression [38, 41]. Under hypoxia, tumor cells secrete vascular endothelial growth factors (VEGF), which stimulate angiogenic sprouting. Owen et al.[42] used a mathematical model to capture the interplay between VEGF and oxygen on angiogenesis in tumor tissues. However, severe hypoxia facilitates tumor necrosis. Several mathematical models have been proposed to elucidate the role of tumor necrosis in its progression and therapeutic outcome [39, 43]. Recently, Murphy et al. [37] utilized a mathematical model to illustrate how tumors adapt their growth mechanisms to changing oxygen levels. Recent experimental studies indicate that oxygen level inside the tumor may be able to induce EMT, with low oxygen levels stimulating epithelial cells to acquire mesenchymal characteristics and normoxic conditions reversing this trend [44]. Oxygen heterogeneity is a well-established feature in solid tumors. Hence, it would be worthful to study how oxygen heterogeneity impacts the EMT dynamic in the solid tumor.

In this article, we propose a continuum mathematical model to unfold the missing link between oxygen heterogeneity and the epithelial-mesenchymal transition in the solid tumor. Here, we consider a system of coupled PDEs for the variables mesenchymal, epithelial, dead cell densities, and oxygen concentration. Since mesenchymal cells acquire that ability to move, the proposed model allows mesenchymal cells to be motile. As epithelial cells are tightly connected with each other, we assume that epithelial cells are unable to move. The key difference between the well-known go-or-grow tumor models [29, 32, 45] and our proposed model is that both types of live cells proliferate, which is the main difference with the go-grow hypothesis. Our model distinguishes two extreme phenotypes: epithelial and mesenchymal, and assumes that only mesenchymal cells are motile. In practice, however, within heterogeneous clusters of epithelial and mesenchymal cells, collective movement of both epithelial and mesenchymal cells has been observed [46, 47].

1.1. Layout of the article

We start with a detailed description of the proposed mathematical model in Section 2. To make the model general, we put the model in dimensionless form in Section 3. The simulation methodology is illustrated in Section 3.2. In the next section, we write down the outcome of the simulation-driven results of the proposed model in Section 4. Finally, we devote a discussion of the present work and identify the future direction in Section 5.

2. Mathematical model

In this section, we describe how spatio-temporal changes of the mesenchymal cell density $m(x,t)$, epithelial cell density $e(x,t)$, dead cells density $n(x,t)$, and oxygen concentration $c(x,t)$ are involved in the dynamics of the EMT and derive partial differential equations governing the evolution of each variable, where x denotes the spatial position and t represents time. The schematic diagram is presented in Figure 1.

(a) Mesenchymal cells:

We assume that the density of mesenchymal cells changes due to the dispersion that results from random locomotion, and we choose D_m as the random cell motility coefficient, characterizing how the cells would disperse from higher to lower densities. Mesenchymal cells proliferate at the rate r_m when the oxygen concentration is above the critical value of c_1. Epithelial cells are transferred to the mesenchymal phenotype at a rate r_{em} when oxygen concentration falls below the critical

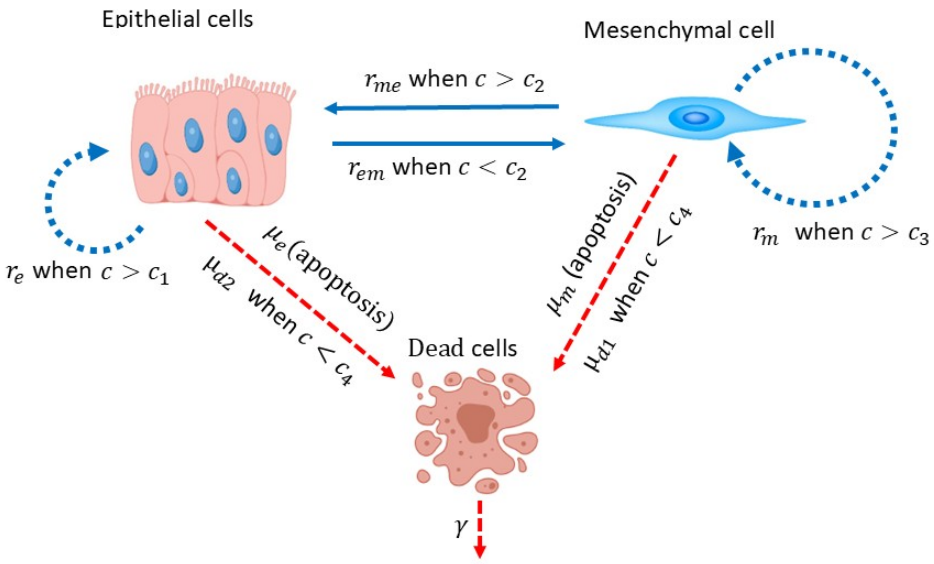

Figure 1: Schematic showing the interactions between epithelial, mesenchymal, and dead cells, e, m, n, respectively, in response to oxygen concentration c during the EMT process.

value c_2. However, mesenchymal cells turn into epithelial cells again when the oxygen level is raised above c_2. Mesenchymal cells die at the rate μ_m.

To summarize, the spatio-temporal evolution of mesenchymal cell density leads to the differential equation (using mass conservation law),

$$\frac{\partial m}{\partial t} = \underbrace{D_m \frac{\partial^2 m}{\partial x^2}}_{motility} + \underbrace{r_m m(1 - \frac{m+e+n}{K})H(c-c_1)}_{proliferation} + \underbrace{r_{em}(1+\theta\frac{m}{K})eH(c_2-c)}_{E\ to\ M\ under\ influence\ of\ M} \tag{1}$$
$$- \underbrace{r_{me}(1-\delta\frac{m}{K})mH(c-c_2)}_{M\ to\ E\ under\ influence\ of\ M} - \underbrace{\mu_m m}_{apoptosis} - \underbrace{\mu_{d_1} m H(c_4-c)}_{necrotic\ death},$$

where K is the carrying capacity of tumor. The second term on the right-hand side (RHS) of Eq. (1) represents the mesenchymal cells proliferate in the logistic manner with the rate r_m in the environment where oxygen concentration above a threshold value c_1. The third term of RHS denotes epithelial cell changes to the mesenchymal cell with the rate r_{em} when epithelial cells are exposed to the oxygen environment; oxygen concentration falls below c_2, i.e., $c < c_2$, with the influence of mesenchymal cells. θ is the influence parameter. The fourth term of RHS denotes mesenchymal cells back to epithelial with the rate r_{me} when oxygen concentration is above the critical value c_2. However, this transition is resisted by mesenchymal cells with the parameter δ. The fifth term accounts for mesenchymal cell death at the constant rate μ_m. The last term on the RHS indicates

that the mesenchymal cells die at a rate μ_{d_1} when c falls below the necrotic threshold value c_4.

(b) Epithelial cells:

Experimental evidence shows that epithelial cells are attached through highly adhesive molecules. So, we assume that epithelial cells are not motile. Epithelial cells proliferate when oxygen concentration is above the threshold value c_3. When oxygen concentration $c > c_2$, mesenchymal cells regain epithelial phenotype. Therefore, the third term in Eq. (1) acts as a source term for epithelial cell density. Epithelial cells transient into mesenchymal cells under the influence of mesenchymal cells. Hence, the second term of Eq. (1) acts as a sink term. To summarize, the mass conservation for epithelial cells is applied, which gives

$$\begin{aligned}\frac{\partial e}{\partial t} =& \underbrace{r_e e(1-\frac{m+e+n}{K})H(c-c_3)}_{proliferation} + \underbrace{r_{me}(1-\delta\frac{m}{K})mH(c-c_2)}_{M\ to\ E\ under\ influence\ of\ M} \\ &- \underbrace{r_{em}(1+\theta\frac{m}{K})eH(c_2-c)}_{E\ to\ M\ under\ influence\ of\ M} - \underbrace{\mu_e e}_{apoptosis} - \underbrace{\mu_{d_2} eH(c_4-c)}_{necrotic\ death},\end{aligned} \tag{2}$$

where r_e denotes the proliferation rate of epithelial cells and μ_e represents the death rate of epithelial cells.

Since mesenchymal cells can proliferate in lower oxygen environments than epithelial cells, we assume that $c_1 \leq c_3$. EMT is initiated when the oxygen level falls below the threshold for mesenchymal cell proliferation, i.e., where $c < c_2 < c_1$. The threshold value for necrosis is smaller than the EMT threshold value, i.e, $c_4 < c_2$. Therefore, the ordering of the various oxygen thresholds can be summarized as $c_4 < c_2 < c_1 \leq c_3$.

(c) Dead cells:

Dead cells are generated in various ways. The most common ways are cellular program death and cellular death due to a shortage of oxygen. Also, dead cells undergo natural decay with a rate γ_1.

$$\frac{\partial n}{\partial t} = \mu_m m + \mu_e e + \mu_{d_1} mH(c_4-c) + \mu_{d_2} eH(c_4-c) - \underbrace{\gamma n}_{decay}, \tag{3}$$

(d) Oxygen concentration:

Cells need nutrients and oxygen to sustain life. In our study, oxygen is taken as a pivotal element for a cell's metabolic element. Oxygen is consumed by epithelial and mesenchymal cells. These consumption terms can be non-linear. However, we assume that oxygen is consumed linearly by epithelial and mesenchymal cells. The oxygen reaction-diffusion equation is given as,

$$\frac{\partial c}{\partial t} = D_c\frac{\partial^2 c}{\partial x^2} - \underbrace{\lambda_e ce}_{consumption\ by\ E} - \underbrace{\lambda_m cm}_{consumption\ by\ M}, \tag{4}$$

where λ_e and λ_m represent the oxygen consumption rates for epithelial and mesenchymal cells, respectively. D_c denotes the diffusion coefficient of oxygen.

Hence, the complete system of equations describing the interactions between the mesenchymal

cell density, epithelial cell density, dead cell density, and oxygen concentration are given as:

$$\begin{aligned}
\frac{\partial m}{\partial t} &= D_m \frac{\partial^2 m}{\partial x^2} + r_m m(1 - \frac{m+e+n}{K})H(c-c_1) + r_{em}(1+\theta\frac{m}{K})eH(c_2-c) - \\
&\quad r_{me}(1-\delta\frac{m}{K})mH(c-c_2) - \mu_m m - \mu_{d_1} mH(c_4-c), \\
\frac{\partial e}{\partial t} &= r_e e(1 - \frac{m+e+n}{K})H(c-c_3) + r_{me}(1-\delta\frac{m}{K})mH(c-c_2) - r_{em}(1+\theta\frac{m}{K})eH(c_2-c) \\
&\quad - \mu_e e - \mu_{d_2} eH(c_4-c), \\
\frac{\partial n}{\partial t} &= \mu_m m + \mu_e e + \mu_{d_1} mH(c_4-c) + \mu_{d_2} eH(c_4-c) - \gamma n, \\
\frac{\partial c}{\partial t} &= D_c \frac{\partial^2 c}{\partial x^2} - \lambda_e ce - \lambda_m cm.
\end{aligned} \tag{5}$$

Table 1: Parameter description.

Parameter	Description
D_m	Diffusion coefficients of mesenchymal cells
r_m	Proliferation rate of mesenchymal cells
K	Carrying capacity
r_e	Proliferation rate of epithelial cells
r_{em}	Transition rate from E to M
r_{me}	Transition rate from M to E
θ	Influence of mesenchymal cells on E to M transition
δ	Influence of mesenchymal cells to reduce M-E transition
c_1	Critical value of oxygen concentration is required for mesenchymal cell proliferation
c_2	Critical value of oxygen concentration required for M to E transition
c_3	Critical value of oxygen concentration is required for epithelial cell proliferation
c_4	Critical value of oxygen concentration for necrosis
μ_m	Apoptotic death rate of mesenchymal cells
μ_e	Apoptotic death rate of epithelial cells
μ_{d_1}	Necrotic death rate of mesenchymal cells
μ_{d_2}	Necrotic death rate of epithelial cells
D_c	Diffusion coefficients of oxygen
λ_e	Oxygen consumption rate by epithelial cells
λ_m	Oxygen consumption rate by mesenchymal cells

2.1. Initial and boundary condition

To close the system, the initial and boundary conditions need to be prescribed for m, e, n, and c.

Boundary conditions: We assume "no flux" boundary condition for mesenchymal cells at both the boundaries, namely $x = 0$ and $x = L$. Oxygen concentration at $x = 0$ is assumed to be a symmetric boundary condition, and it is assumed that oxygen is supplied to the system through the boundary $x = L$ with a constant rate c_∞. Hence, these conditions are given as,

$$\frac{\partial m}{\partial x} = \frac{\partial c}{\partial x} = 0 \text{ at } x = 0 \,\forall\, t > 0, \tag{6}$$

$$\frac{\partial m}{\partial x} = 0,\ c = c_\infty \text{ at } x = L \,\forall\, t > 0. \tag{7}$$

Initial conditions: We assume that oxygen initially is available at a sufficient amount throughout the domain. It is considered that the oxygen concentration is same as that at the boundary ($x = L$). In *in vitro* study, the experiment is conducted with fewer mesenchymal cells than epithelial cells. Hence, the initial conditions are posed as

$$m(x,0) = A\exp(-\frac{x^2}{\epsilon}),\ e(x,0) = B\exp(-\frac{x^2}{\epsilon}),\ n(x,0) = 0, \text{ and } c(x,0) = c_\infty, \text{ with } \epsilon = 0.01, \tag{8}$$

where A and B denote the initial densities of mesenchymal and epithelial cells, respectively, with $A < B$.

3. Non-dimensionalization

To put the model in a non-dimensional form, we follow the standard methodology. The reference time scale (τ) is the time value for mitotic cell division of mesenchymal cells. Therefore, $\tau = \frac{1}{r_m}\ day$. The characteristic length (X) is taken to be equal to $\sqrt{D_c\tau}$. The characteristic value of oxygen concentration is considered to be the same as that of oxygen supplied at the boundary. Using bar to denote dimensionless variables, we set

$$\bar{t} = \frac{t}{\tau},\ \bar{x} = \frac{x}{X},\ \bar{e} = \frac{e}{K},\ \bar{m} = \frac{m}{K}, \text{ and } \bar{c} = \frac{c}{c_\infty}. \tag{9}$$

The non-dimensional model is given as (dropping bar from the variables)

$$\begin{aligned}\frac{\partial m}{\partial t} &= D_m^*\frac{\partial^2 m}{\partial x^2} + m(1-m-e-n)H(c-c_1^*) + r_{em}^*(1+\theta m)eH(c_2^*-c) - \\ &\quad r_{me}^*(1-\delta m)mH(c-c_2^*) - \mu_m^* m - \mu_{d_1}^* mH(c_4^*-c),\end{aligned} \tag{10}$$

$$\begin{aligned}\frac{\partial e}{\partial t} &= r_e^* e(1-m-e-n)H(c-c_3^*) - r_{em}^*(1+\theta m)eH(c_2^*-c) + \\ &\quad r_{me}^*(1-\delta m)mH(c-c_2^*) - \mu_e^* e - \mu_{d_2}^* eH(c_4^*-c),\end{aligned} \tag{11}$$

$$\frac{\partial n}{\partial t} = \mu_m^* m + \mu_e^* e + \mu_{d_1}^* mH(c_4^*-c) + \mu_{d_2}^* eH(c_4^*-c) - \gamma_1^* n, \tag{12}$$

$$\frac{\partial c}{\partial t} = \frac{\partial^2 c}{\partial x^2} - \lambda_e^* ce - \lambda_m^* cm. \tag{13}$$

The boundary conditions for the governing equations are given as

$$\frac{\partial c}{\partial x} = 0 \text{ at } x = 0, c(L^*,t) = 1, \tag{14}$$

$$\frac{\partial m}{\partial x} = 0 \text{ at } x = 0, L^*,\ \forall t > 0. \tag{15}$$

The initial conditions are considered as

$$m(x,0) = A^* \exp(-\frac{x^2}{\epsilon}),\ e(x,0) = B^* \exp(-\frac{x^2}{\epsilon}),\ n(x,0) = 0,\ \text{and}\ c(x,0) = 1 \text{ in } [0, L^*]. \quad (16)$$

The non-dimensional parameter groups introduced into Eqs. (10)-(13) are defined below as

$$D_m^* = \frac{D_m}{D_c}, r_e^* = \tau r_e, r_{em}^* = \tau r_{em}, r_{me}^* = \tau r_{me}, \mu_m^* = \tau \mu_m, \mu_e^* = \tau \mu_e K, \lambda_m^* = \tau \lambda_m K,$$
$$\lambda_e^* = \tau \lambda_e, L^* = \frac{L}{X}, \gamma^* = \gamma \tau, A^* = \frac{A}{K} \text{ and } B^* = \frac{B}{K}.$$

3.1. Parameter choice

Since no single experiment estimated all the parameter values, we collect the parameter values from the existing literature. The value of oxygen diffusivity inside the tumor is taken as $2 \times 10^{-9}\ m^2 s^{-1}$ [48]. The diffusivity of mesenchymal tumor cells lies in the range $1 \times 10^{-15} - 0.75 \times 10^{-11}\ m^2 s^{-1}$ [49, 50]. Various experimental studies suggest that the proliferation rate of epithelial cells is faster than that of mesenchymal cells [51]. Suzuki et al. [52]experimentally showed that the epithelial cell proliferation rate is up to 3.6 times the mesenchymal cell proliferation rate. Parameters $r_m = 0.44\ day^{-1}$, $r_e = 1.38\ day^{-1}$, $r_{em} = 0.36 - 0.45\ day^{-1}$, $= 0.156 - 0.2\ day^{-1}$ [53, 54, 55, 51]. The value of characteristic length (X) is $1.97 \times 10^{-2}\ cm$. The value of c_4 is $1.7\ mmHg$, $c_\infty = 10 - 20\ mmHg$ [56]. Mesenchymal cells consume oxygen at a maximum rate that varies in the range $0.1 - 3\ pmol\ h^{-1} cell^{-1}$ [57, 58]. The apoptotic death rates for epithelial cells (μ_e) and mesenchymal cells (μ_m) are taken $0.054\ day^{-1}$ and $0.054\ day^{-1}$, respectively, which belong to the range given in [59].

Table 2 shows the dimensionless parameter values.

3.2. Numerical simulation method

In order to solve numerically, the governing equations (10)-(13) subject to the initial conditions (16)and boundary conditions (14)-(15) over the domain $[0, L^*]$ are discretized in finite difference framework using implicit forward time and central space (FTCS) scheme. The domain $[0, L^*]$ is partitioned into $(N-1)$ number sub-interval into equal width Δx. Therefore, $\Delta x = \frac{L^*}{(N-1)}$. We carry out simulation up to T_{final}. To march the final time T_{final}, we chose Δt as the time step length for P times. So, $\Delta t = \frac{T_{final}}{P}$. We denote $m(i\Delta x, k\Delta t) = m_i^k$, $e(i\Delta x, k\Delta t) = e_i^k$, $n(i\Delta x, k\Delta t) = n_i^k$, and $c(i\Delta x, k\Delta t) = c_i^k$, where $i = 0, \ldots, N-1$ and $k = 0, \ldots, P$.

The resulted difference equation for Eq. (10) is obtained as

$$\begin{aligned} -D_1 m_{i-1}^{k+1} + (1+2D_1) m_i^{k+1} - D_1 m_{i+1}^{k+1} = m_i^k + \Delta t (& m_i^k (1 - m_i^k - e_i^k - n_i^k) H(c_i^k - c_1^*) \\ & + r_{em}^* (1 + \theta m_i^k) e_i^k H(c_2^* - c_i^k) H(c_i^k - c_4^*) - r_{me}^* (1 - \delta m_i^k) m H(c_i^k - c_2^*) \\ & - \mu_m^* m_i^k - \mu_{d_1}^* m_i^k H(c_4^* - c_i^k)), \end{aligned} \quad (17)$$

which is valid for $i = 1, \ldots, N-2$ and $k = 0, 1, \ldots, P$. Here $D_1 = \frac{\Delta t D_m^*}{\Delta x^2}$.
At boundary nodes (i.e., $i = 0, N-1$), by employing no-flux boundary condition, the difference

Table 2: Dimensionless parameter values.

Parameter	Base value	Range
D_m^*	3.75×10^{-5}	$5 \times 10^{-7} - 3.75 \times 10^{-3}$
r_m^*	1	
r_e^*	3.5	
r_{em}^*	0.75	$0.674 - 0.9675$
r_{me}^*	0.43	$0.335 - 0.43$
μ_m^*	0.065	
μ_e^*	0.095	
δ	0.5	$0 - 1$
θ	3	$1 - 4$
λ_e^*	2.5	
λ_m^*	2.5	
c_1^*	0.6	
c_2^*	0.5	
c_3^*	0.6	
c_4^*	0.17	
γ^*	0.02	
$\mu_{d_1}^*$	0.022	
$\mu_{d_2}^*$	0.022	
A^*	0.2	
B^*	0.8	
L^*	2.54	–

equations for Eq. (10) are obtained as

$$
\begin{aligned}
&(1+2D_1)m_0^{k+1} - 2D_1 m_1^{k+1} = m_0^k + \Delta t(m_0^k(1 - m_0^k - e_0^k - n_0^k)H(c_0^k - c_1^*) \\
&+ r_{em}^*(1+\theta m_0^k)e_i^k H(c_2^* - c_0^k)H(c_0^k - c_4^*) - r_{me}^*(1-\delta m_0^k)mH(c_0^k - c_2^*) \\
&- \mu_m^* m_0^k - \mu_{d_1}^* m_0^k H(c_4^* - c_0^k)), \qquad (18) \\
&- 2D_1 m_{N-2}^{k+1} + (1+2D_1)m_{N-1}^{k+1} = m_{N-1}^k + \Delta t(m_{N-1}^k(1 - m_{N-1}^k - e_{N-1}^k - n_{N-1}^k)H(c_{N-1}^k - c_1^*) \\
&+ r_{em}^*(1+\theta m_{N-1}^k)e_{N-1}^k H(c_2^* - c_{N-1}^k)H(c_{N-1}^k - c_4^*) - r_{me}^*(1-\delta m_{N-1}^k)mH(c_{N-1}^k - c_2^*) \\
&- \mu_m^* m_{N-1}^k - \mu_{d_1}^* m_{N-1}^k H(c_4^* - c_{N-1}^k)). \qquad (19)
\end{aligned}
$$

Eqs. (11) and (12) are discretized respectively as,

$$
\begin{aligned}
e_i^{k+1} &= e_i^k + \Delta t(r_e^* e_i^k(1 - m_i^k - e_i^k - n_i^k)H(c_i^k - c_3^*) - r_{em}^*(1+\theta m_i^k)e_i^k H(c_2^* - c_i^k)H(c_i^k - c_4^*) \\
&\quad + r_{me}^*(1-\delta m_i^k)mH(c_i^k - c_2^*) - \mu_e^* e_i^k - \mu_{d_2}^* e_i^k H(c_4^* - c_i^k)), \qquad (20) \\
n_i^{k+1} &= \mu_m^* m_i^k + \mu_e^* e_i^k + \mu_{d_1}^* m_i^k H(c_4^* - c) + \mu_{d_2}^* e_i^k H(c_4^* - c) - \gamma^* n_i^k, \qquad (21)
\end{aligned}
$$

which is valid for all spatial grid points.
The oxygen diffusion equation (13) is discretized as,

$$
-D_2 c_{i-1}^{k+1} + (1+2D_2)c_i^{k+1} - D_2 c_{i+1}^{k+1} = c_i^k - \Delta t c_i^k(\lambda_e e_i^k + \lambda_m m_i^k), \qquad (22)
$$

which is applicable for the grid points $i = 1, \ldots, N-3$ with $D_2 = \frac{\Delta t}{\Delta x^2}$.
At the boundary node $i = 0$, by deploying no-flux boundary condition, the discretized form of Eq. (13) is given as,

$$(1 + 2D_2)c_0^{k+1} - 2D_2 c_1^{k+1} = c_0^k - \Delta t c_0^k(\lambda_e e_0^k + \lambda_m m_0^k). \tag{23}$$

At the node $i = N-2$, the finite difference equation of Eq. (13) takes form as follows,

$$-D_2 c_{N-3}^{k+1} + (1 + 2D_2)c_{N-2}^{k+1} = D_2 + c_i^k - \Delta t c_{N-2}^k(\lambda_e e_{N-2}^k + \lambda_m m_{N-2}^k). \tag{24}$$

The numerical algorithm is implemented in C, and mesh independence was tested before numerical simulations were performed. In this case, we fix $N = 1001$, $P = 24 \times 10^4$ and $D_2 = 77.5$. Note that the forward-time central-space (FTCS) implicit scheme in the finite difference framework is used to discretize the model equations, and it is unconditionally convergent [60].

4. Numerical results

Here, we simulate the proposed model up to dimensionless time $T_{final} = 120$, which corresponds to a dimensional value 90 days. We have used the dimensionless parameter values, shown in Table 2. The total volume ($V_{tot}(t)$) is defined as,

$$V_{tot}(t) = \frac{1}{L_{max}} \int_0^{L_{max}} (m(x,t) + e(x,t) + n(x,t))dx, \tag{25}$$

where L_{max} is the length between the tumor center and the tumor tip point at each time step. $L_{max}(t)$ is calculated using $m(L_{max}(t), t) + e(L_{max}(t), t) + n(L_{max}(t), t) = \eta$ at each time point. Here, we fix $\eta = 10^{-6}$ arbitrarily sufficiently small. Note that our model is formulated in a one-dimensional Cartesian framework. As a result, the tumor volume should be interpreted as the tumor size.
The total volume of epithelial ($E(t)$) and mesenchymal cells ($M(t)$) are defined as,

$$E(t) = \frac{1}{L_{max}} \int_0^{L_{max}} e(x,t)dx \text{ and } M(t) = \frac{1}{L_{max}} \int_0^{L_{max}} m(x,t)dx. \tag{26}$$

Also, the fraction of total live cells is defined as,

$$(\text{fraction of live cells}) = \frac{E(t) + M(t)}{V_{tot}(t)}. \tag{27}$$

The volume fraction of mesenchymal (M_{frac}) and epithelial cell (E_{frac}) are defined as,

$$M_{frac}^{live}(t) = \frac{M(t)}{E(t) + M(t)},\ E_{frac}^{live}(t) = \frac{E(t)}{E(t) + M(t)} \tag{28}$$

$$M_{frac}^{total}(t) = \frac{M(t)}{V_{tot}(t)},\ E_{frac}^{total}(t) = \frac{E(t)}{V_{tot}(t)}, \tag{29}$$

where superscripts *live* and *total* denote the fractions of epithelial and mesenchymal are calculated corresponding to total live cell volume and total tumor volume, respectively.
To estimate the velocity of the tumor tip point, we use the following formula,

$$v(t, t + \delta t) = \frac{L_{max}(t + \delta t) - L_{max}(t)}{\delta t},$$

where δt is the time between two subsequent measurements of the position of the tumor front point (L_{max}).

4.1. In the case where oxygen is uniformly distributed within the tumor domain

In the *in vitro* protocol, tumor cultures are maintained with fixed oxygen levels in the growth medium to study the impact of oxygenation on various biological phenomena, which rely on specific critical thresholds. In this study, we consider that when the oxygen concentration (c) falls below c_2^*, the epithelial-mesenchymal transition begins and when the oxygen level is above c_2^*, the reverse epithelial-mesenchymal transition begins. In addition, fluctuation in oxygen is a common feature in the microenvironment of a real tumor. This biological characteristic can be mimicked in the *in vitro* setup by controlling oxygen supply in tumor culture medium [61]. Experimental studies show that necrotic materials are released from the tumor region and appear on the surface of the culture medium. Therefore, the competition for space between epithelial and mesenchymal cells is considered. Hence, the governing equations are redefined as

$$\begin{aligned}\frac{\partial m}{\partial t} &= D_m^* \frac{\partial^2 m}{\partial x^2} + m(1-m-e)H(c-c_1^*) + r_{em}^*(1+\theta m)eH(c_2^*-c)H(c-c_4^*) - \\ &\quad r_{me}^*(1-\delta m)mH(c-c_2^*) - \mu_m^* m - \mu_{d_1}^* mH(c_4^*-c), \qquad (30)\\ \frac{\partial e}{\partial t} &= r_e^* e(1-m-e)H(c-c_3^*) - r_{em}^*(1+\theta m)eH(c_2^*-c)H(c-c_4^*) + \\ &\quad r_{me}^*(1-\delta m)mH(c-c_2^*) - \mu_e^* e - \mu_{d_2}^* eH(c_4^*-c), \qquad (31)\end{aligned}$$

where the oxygen levels ($c = c(t)$) (where t is time) are assumed to be spatially homogeneous. Figure 2 shows two protocols. In the first case, the oxygen field in the culture medium is greater than c_2^* or less than c_2^*. On the other hand, oxygen fields change to $c > c_2^*$ for the first half and at the other half to $c < c_2^*$, and vice versa.

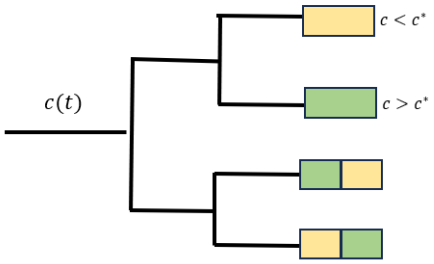

Figure 2: Schematic representation of oxygen levels distribute spatially homogeneous in the tumor growth medium. The green colour denotes $c > c_2^*$, and the yellow colour denotes $c < c_2^*$. The branches are split into two categories, the culture medium is either greater than or less than c_2^* through the culture time, and the other one is at the first half time of the course of the simulation, $c(t) > c_2^*$ and on the last half of it, $c(t) < c_2^*$, and vice-versa.

4.1.1. When the oxygen concentration in the growth medium has a higher value than critical oxygen concentration of the mesenchymal-to-epithelial transition i.e., $c > c_2^*$ uniformly

We consider that the oxygen level is fixed at $c = 0.7$ ($> c_2^*$) in the tumor culture medium. Figure 3a reveals that after a very initial short time, the tumor consisting of the epithelial and mesenchymal cell population converts into an epithelial tumor. As per the culture medium's oxygen level, mesenchymal cells immediately turn into epithelial phenotype. Epithelial cells do not have motile characteristics. Hence, no spatial advancement of the tumor is observed. It highlights the significant impact of oxygen levels on the phenotypic switch of tumor populations. In this case, the entire tumor turns into an epithelial kind.

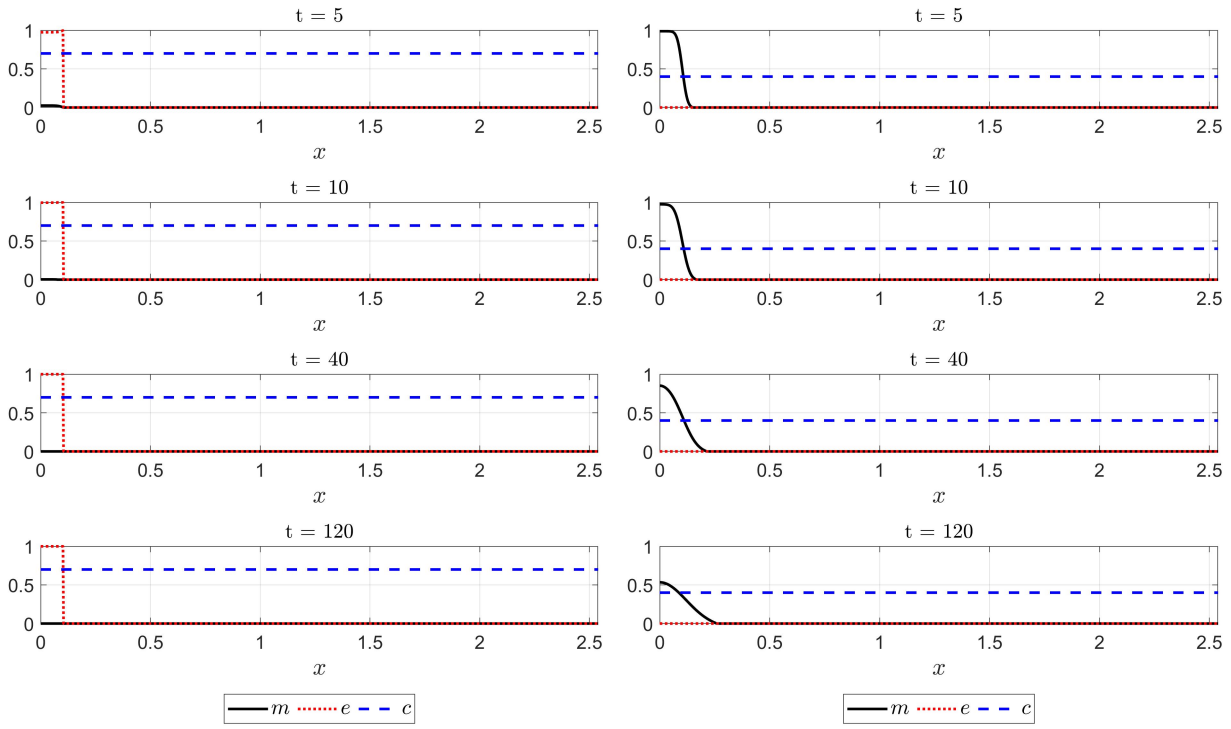

Figure 3: When the tumor grows in a medium with a spatially uniform oxygen level of $c = 0.7$ in Figure (a) and $c = 0.4$ in Figure (b), results are obtained by solving Eqs. (30) and (31) with compact support initial conditions: $m(x, 0) = 0.2$ and $e(x, 0) = 0.8$ for $x \in [0, 0.2] \subset [0, L^*]$. The remaining parameters are listed in Table 2.

4.1.2. When oxygen concentration has a lower value than critical oxygen concentration of the mesenchymal-to-epithelial transition i.e., $c < c_2^*$ in the tumor medium

In this case, we mimic the condition in which tumor cultures are in fixed oxygen medium lower than the critical oxygen level to switch the epithelial to mesenchymal transition. In Figure 3b, it can be seen that the tumor only has a mesenchymal cell population after the initial transition time. Since the oxygen level is below the oxygen proliferation threshold value, it is evident that mesenchymal cells cannot proliferate. As a result, the density of mesenchymal cells decreases. Moreover, it is observed that the tumor spatially expands as the mesenchymal cells have a motility feature.

4.1.3. When tumor exposed in $c > c_2^*$ up to $t = 60$ initially, later on tumor grows in the environment $c < c_2^*$

The oxygen level is maintained above c_2^* up to $t = 60$. After this time, the oxygen level is fixed at a lower value of c_2^*. This, in silico condition, mimics the situation in which the tumor is cultured at a high oxygen level, and after a certain time period, the tumor shifts to a growth environment of a lower oxygen level. Figure 4a illustrates that when the tumor grows in $c = 0.7(> c_2^*)$, the tumor consists only of epithelial cells except for the initial transient periods of growth. However, in the growth circumstance $c < c_2^*$, that is, after $t = 60$ onward, the tumor changes all its epithelial population into a mesenchymal phenotype.

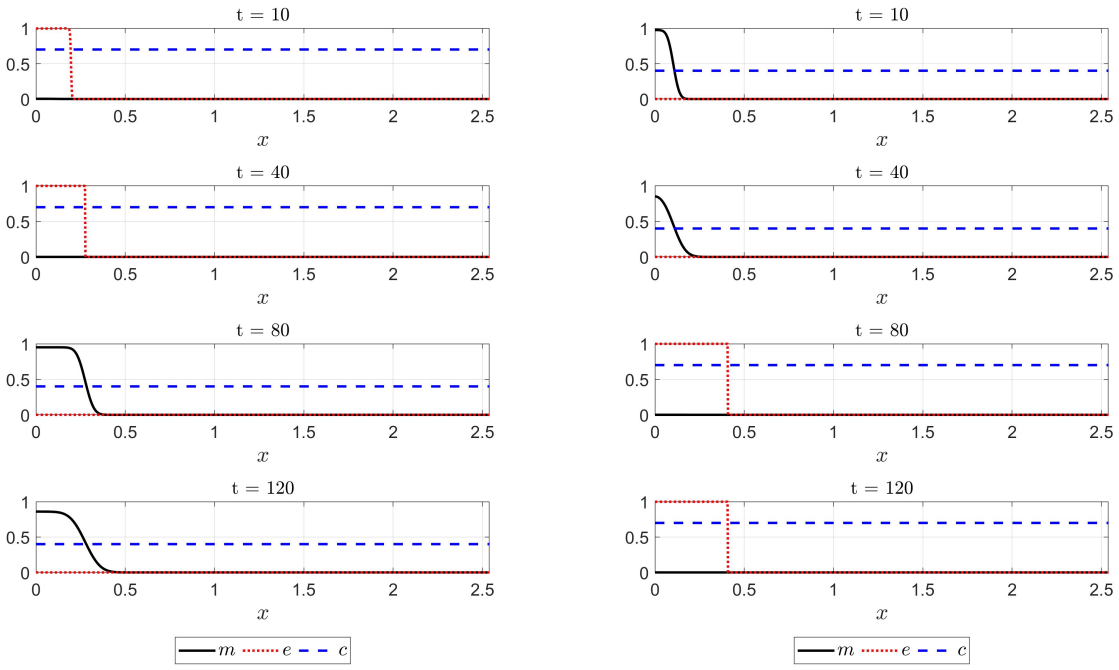

(a) (b)

Figure 4: The spatial distribution of epithelial and mesenchymal cell densities at times $t = 10, 40, 80$, and 120 when the oxygen concentration is kept at $c = 0.7$ from the initial time to $t = 60$, after which it remains at $c = 0.4$ for the rest of the simulation in (a) and when $c = 0.4$ for initial $t = 60$ and later stage oxygen levels set at $c = 0.7$ in (b). To obtain these results, Eqs. (30) and (31) are simulated with compact support initial conditions: $m(x, 0) = 0.2$ and $e(x, 0) = 0.8$ for $x \in [0, 0.2] \subset [0, L^*]$.

4.1.4. When tumor exposed in $c < c_2^*$ up to $t = 60$ initially, later on tumor grows in the environment $c > c_2^*$

In this case, we let the tumor grow in a medium with $c < c_2^*$ for the first half of the growth period, and then the tumor is placed into a medium with an oxygen level of $c > c_2^*$ for the remaining duration.

Figure 4b displays the spatial distribution of mesenchymal and epithelial cells for various time stages $t = 10, 40, 80$ and 120. One can observe that when the growth medium has an oxygen level $c < c_2^*$, the tumor consists only of cells of the mesenchymal phenotype before the culture medium sifts into a higher oxygen level, that is $c > c_2^*$. The qualitative behavior is the same as in the previous case. However, in this case, the tumor appears as an epithelial kind.

From all of the above cases, it is concluded that tumor populations switch into a single type sub-population depending on the oxygen level in the growth medium. However, it is interesting to observe that tumor culture in the settings $c < c_2^*$ in the first time interval and in the remaining time $c > c_2^*$, the tumor volume ended with a high value compared to the tumor volume in the culture setting $c > c_2^*$ in the first time interval and in the remaining time $c < c_2^*$ (results are not shown). In addition, it is also observed that when the culture medium changes at the time point $t = 60$, the tumor takes more time to convert all mesenchymal populations into a complete epithelial phenotype when the growth medium changes from $c < c_2^*$ to $c > c_2^*$ compared to the time it takes for the epithelial population tumor to switch to a complete mesenchymal phenotype when the growth environment changes from $c > c_2^*$ to $c < c_2^*$ (Figure 5b). Experimental studies

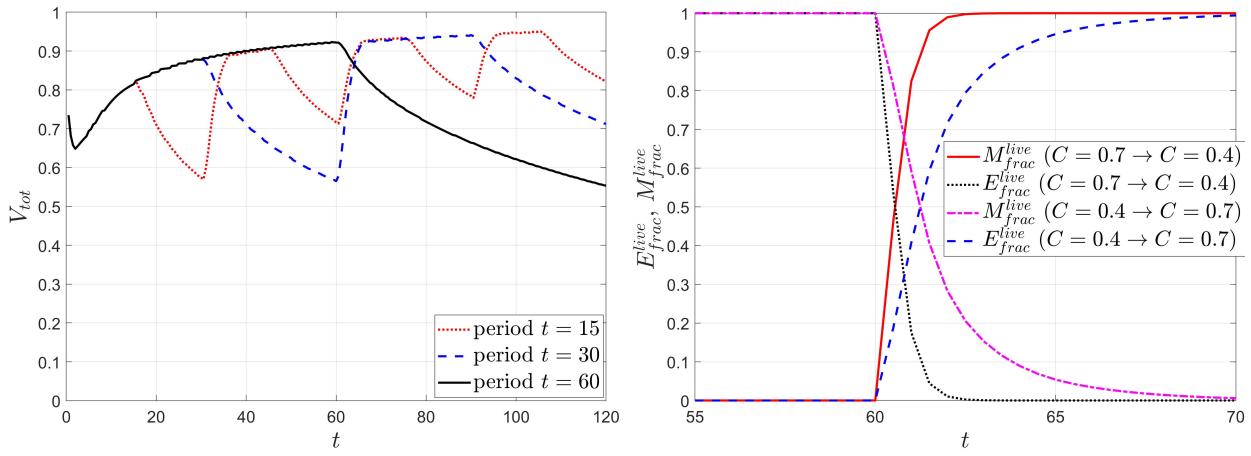

(a) (b)

Figure 5: (a) represents total tumor volume evolution over time in the case when oxygen concentration $c > c^*$ changes to $c < c^*$ periodically at different periods $t = 15, 30$, and 60. (b) illustrates the time evolution of the volume fractions of epithelial and mesenchymal cells, respectively, for two cases: (i) the oxygen concentration is kept at $c = 0.7$ from the initial time to $t = 60$, after which it remains at $c = 0.4$ for the rest of the time; and (ii) the oxygen concentration is kept at $c = 0.4$ from the initial time to $t = 60$, after which it remains at $c = 0.7$ for the rest of the time.

showed that the time scale of oxygen fluctuation at the tumor site has a wide range [62]. Inspired by this observation, we further investigate whether the more frequent switch from a high-oxygen environment into a low-oxygen environment impacts the tumor volume and tumor dynamics. We performed simulations for different values of the oxygen environment switching time periods, e.g., $t = 15, 30$, and 60. Figure 5a shows the evolution of tumor volume over time when the tumor is initially exposed to a culture medium of higher oxygen ($c > c_2^*$) and then transferred to a medium of lower oxygen ($c < c_2^*$) in a periodic manner with time periods of $t = 15, 30$ and 60. In a time interval, the tumor is in a high oxygen culture medium; the tumor converts into an epithelial type. However, in the next time interval, when the tumor is in a low oxygen culture medium, the tumor becomes a mesenchymal one and is spatially spared in nature (the results are not shown). However, one can see that the total volume increases in rapid oxygen fluctuation. In shorter periodic oxygen time, the tumor is exposed to oxygen levels, not for a long time at once, enabling the tumor to sustain rapid proliferation in between shifts into two consecutive low oxygen culture mediums (Figure 5a). In the case of an oxygen-fluctuating environment, starting with a low-oxygen field ($c < c_2$) and time periods of $t = 15, 30$, and 60, the time evolution of tumor volume exhibits a qualitative behavior similar to that observed in the previous case. However, by the end of the final simulation time, the tumor volume is higher than in the previous case (results not shown).

4.2. Effects of spatial oxygen heterogeneity on EMT dynamics

Oxygen heterogeneity is a well-established feature in the *in vivo* solid tumor [63]. Oxygen is delivered from the existing blood vessel to the tumor site. As the tumor grows in size, the oxygen gradient starts to develop inside the tumor. As a result, oxygen concentration decreases with increasing distance from the periphery to the center of the tumor. Oxygen level falls to such a level that cells are no longer live. Therefore, the necrotic region is formed. This heterogeneity of oxygen in the tumor triggers various events such as angiogenesis, metabolic adaptation, and alterations in cell phenotype. Here, we investigate how the mesenchymal and epithelial cells and necrotic core

distribution over the domain are impacted by oxygen heterogeneity. This case resembles the *in vivo* scenario. Figure 6 displays the distribution of epithelial, mesenchymal, necrotic cell den-

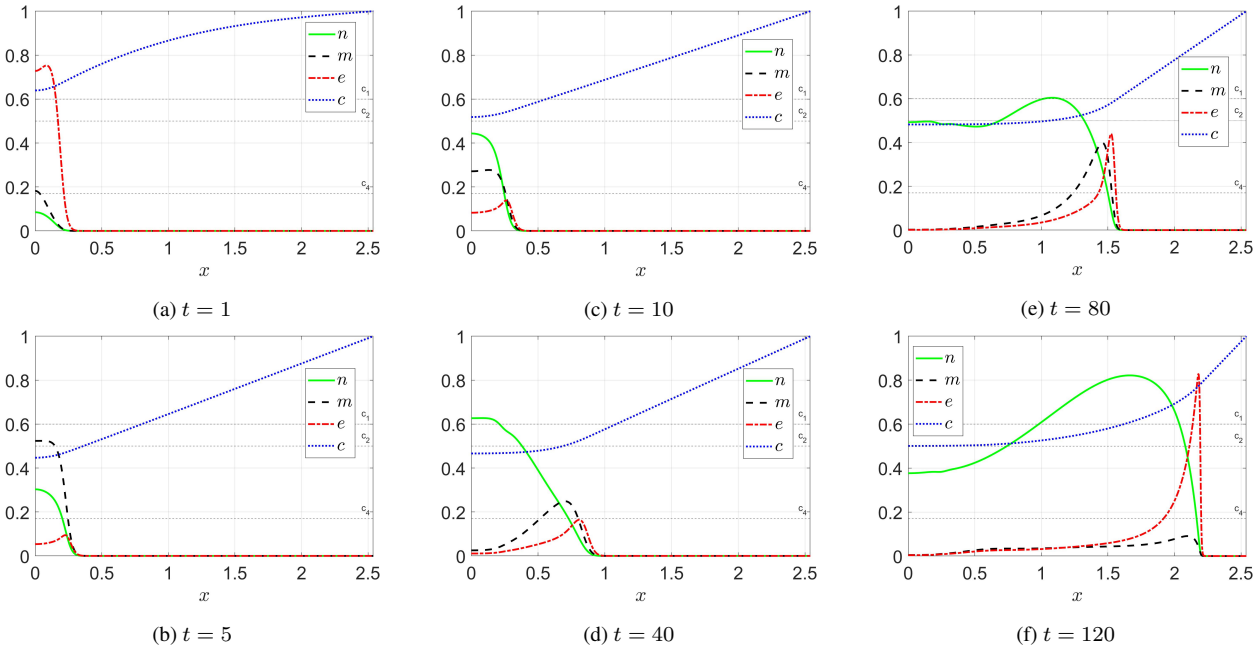

(a) $t = 1$ (c) $t = 10$ (e) $t = 80$

(b) $t = 5$ (d) $t = 40$ (f) $t = 120$

Figure 6: Spatial density profiles for epithelial, mesenchymal, necrotic cells, and oxygen concentration at t=$1, 5, 10, 40, 80$, and 120. The results are obtained by solving model Eqs (10) -(16) using the parameter values in Table 2.

sity, and oxygen concentration in the spatial domain of the tumor at different time levels, such as $t = 1, 5, 10, 20, 40, 80,$ 100 and 120. One can observe that at $t = 1$, the presence of epithelial cell density is higher compared to mesenchymal cell density (Figure 6a). As time progresses gradually, the density of mesenchymal cells increases rapidly. It happens because the oxygen concentration falls below the threshold value of the EMT transition in the tumor domain. The striking thing is that the mesenchymal cells gain the tumor front seat (Figure 6b). However, at subsequent times, epithelial cells appear on the tumor front (Figures 6c-6f). This development is due to the tumor being exposed to a higher oxygen environment where the mesenchymal phenotype population is switched into the epithelial phenotype. Also, it is noticed that a necrotic core is observed to form in the center of the tumor over the course of tumor growth. By $t = 5$, this necrotic core emerges as the dominant feature within the tumor.

The results are shown in Figure 7a, which represents the time evolution of epithelial cells of the volume fraction and live cells volume fraction. It is observed that the volume fraction of epithelial cells with respect to the total volume of the live population decreases in the initial transient time very rapidly. Because in this phase the oxygen level falls below a certain level that only switches from the epithelial phenotype to the mesenchymal phenotype. Later, a spike is noticed. However, toward the end of the simulation, E_{frac}^{live} increases with time. It happens because when a tumor increases its size, the periphery of the tumor is exposed to a higher oxygen level, which is above the cell proliferation threshold. As a result, rapid proliferation of epithelial and mesenchymal cells occurs. Additionally, reverse EMT, i.e., the MET process is activated in this region. All of these collective events lead to an increase in the epithelial volume fraction with respect to the total

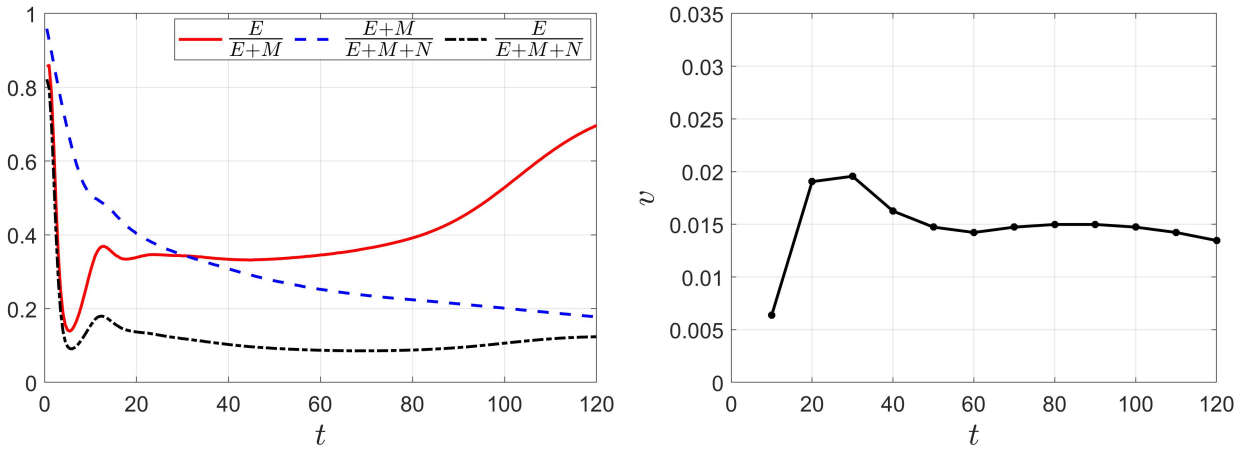

(a) (b)

Figure 7: This figure illustrates (a) the volume fraction of epithelial cell corresponding to total live cell volume and total volume (using the formula Eqs. (28)) and (b) the velocity of the front point of tumor evolution with respect to time.

volume of live cells. The complete mirror results are observed for M_{frac}^{live}. One may note that E_{frac}^{total} and M_{frac}^{total} have qualitative behaviors similar to E_{frac}^{live} and M_{frac}^{live}, respectively. Figure 7b shows the velocity of the tumor front point. This velocity can be interpreted as the speed of the traveling wave in tumor growth dynamics. We observe that the traveling wave approaches to a steady state after an initial transient periods, indicating that the dynamics will remain unchanged over time.

4.3. Effects of diffusivity of mesenchymal cells on EMT process

In this study, live tumor cells are categorized into two cell phenotypes: epithelial and mesenchymal. Experimental studies have established that when epithelial cells acquire a mesenchymal phenotype, mesenchymal cells are exhibited as motile [64]. In this section, we investigate the effects of mesenchymal motility on EMT dynamics and tumor growth in an oxygen-heterogeneous environment. First, we simulate the model, ignoring the effects of mesenchymal cell motility in the simulation. It demonstrates that the distributions are spatially restricted in the initialization domain (results are not shown). However, heterogeneous populations are observed due to the heterogeneous oxygen environment. The effects of different non-zero values of mesenchymal cell motility on mesenchymal, epithelial, and necrotic core distribution are shown in Figure 8. It is noted that we have depicted the results up to $t = 100$. Because the boundary effects appear for the higher value of the motility coefficient, such as for $D_m = 1.15 \times 10^{-4}$. The results show that the pick for epithelial cells is achieved for a higher mesenchymal cell's motility coefficient value. The density of mesenchymal cells increases with time; however, it begins to decay when the tumor size increases. Moreover, one can see that the high value of D_m facilitates the dispersion of epithelial cells. It occurs as the value of D_m increases, the mesenchymal cells migrate to areas where sufficient oxygen is available. In these areas, oxygen levels are adequate to trigger the mesenchymal-epithelial transition (MET) process, allowing mesenchymal cells to adopt epithelial traits. It also leads to the fact that the speed of tumor propagation increases with the increase in D_m (a separate figure for tumor propagation velocity is not shown).

Figure 9 demonstrates the time evolution of M_{frac}^{live} for cases $D_m = 5 \times 10^{-6}$, 3.75×10^{-5}, and

1.15×10^{-4}. It is observed that the volume fraction of mesenchymal cells (M_{frac}^{live}) decreases with time t (when $t > 75$) with the increase in mesenchymal diffusivity D_m. Moreover, M_{frac}^{live} behaves as a rapidly decreasing function for a higher value of D_m. It happens because mesenchymal

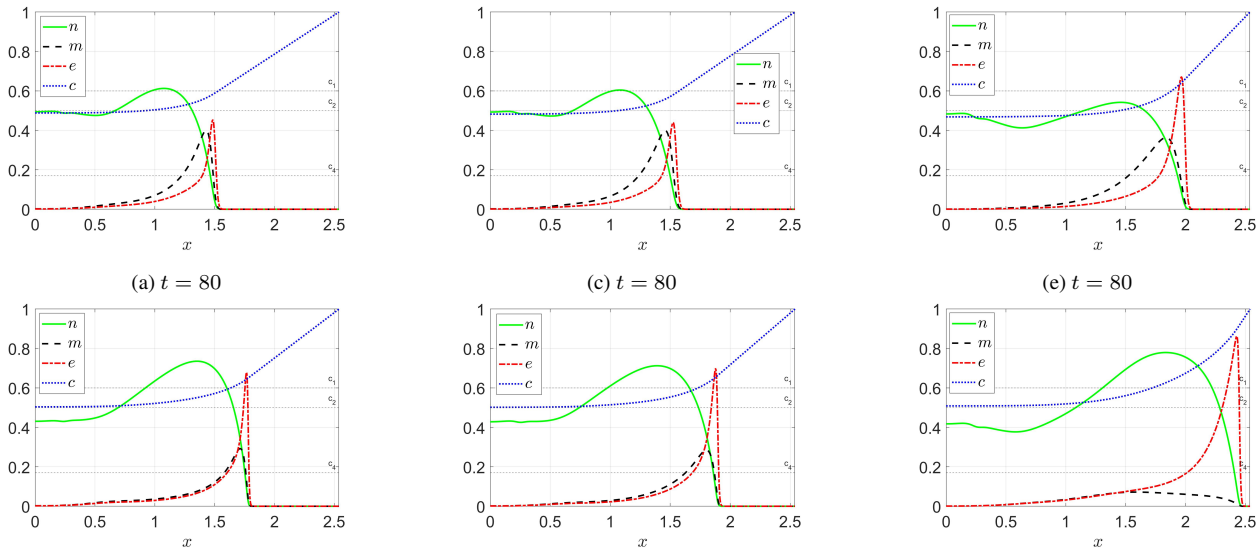

(a) $t = 80$ (c) $t = 80$ (e) $t = 80$

(b) $t = 100$ (d) $t = 100$ (f) $t = 100$

Figure 8: First column for $D_m = 5 \times 10^{-6}$, second column for $D_m = 3.75 \times 10^{-5}$, and third column for $D_m = 1.15 \times 10^{-4}$

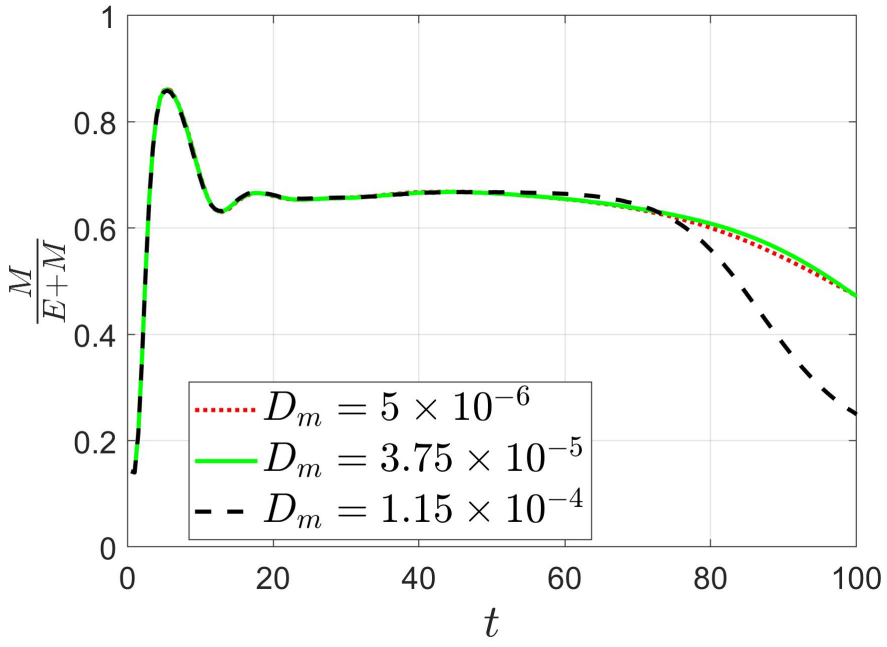

Figure 9: For different values of mesenchymal cell diffusivity, the time evolution of M_{frac}^{live} is displayed.

cells quickly reach the oxygen source site for a higher value of D_m and they are switched into epithelial type immediately. These results highlight a tension between diffusion-driven invasion

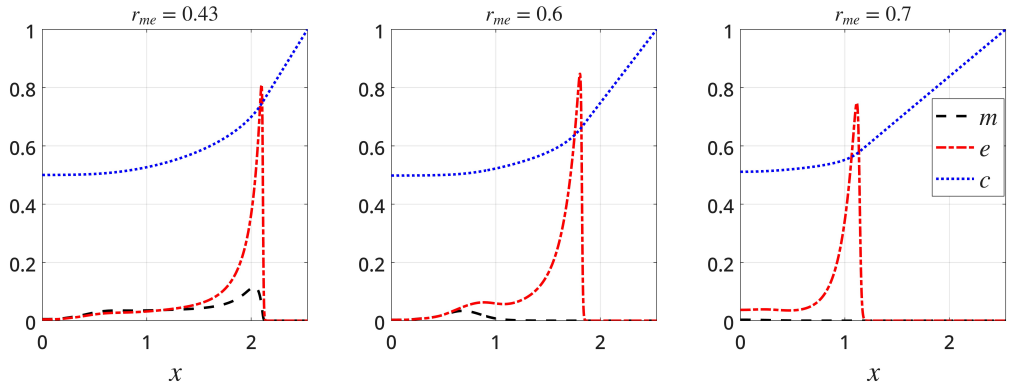

Figure 10: For different values of MET rate r_{me}, the spatial distribution of mesenchymal, epithelial cell densities, and oxygen concentration at $t = 120$. Here, all other parameter values remain the same with Table 2.

and the slowing of growth caused by mesenchymal-to-epithelial transitions (MET). To investigate the extent to which MET restricts invasion, we performed a series of simulations in which we varied the MET rate (r_{me}). As expected, the tumor's invasive potential decreases as the MET rate increases (Figure 10). Therefore, we conclude that stimulating MET by some therapeutic intervention may reduce a tumor's invasiveness.

4.4. Effects of critical oxygen concentration on the proliferation of epithelial and mesenchymal cells on EMT dynamics

Experimental studies have shown that epithelial cells may require a higher oxygen concentration to proliferate compared to mesenchymal cells [44]. In this section, we investigate the impact of the threshold oxygen concentration for mesenchymal and epithelial cell proliferation on EMT dynamics. Here, we consider two cases:

1. The critical oxygen concentration for epithelial cell proliferation is higher than that for mesenchymal cells, i.e., $c_3^* > c_1^*$.

2. Both cell types share the same critical oxygen concentration for proliferation, i.e., $c_3^* = c_1^*$.

Figure 11a demonstrates the temporal evolution of the volume fraction of epithelial cells. It is observed that epithelial cells are present in the tumor in higher amounts for Case 1 compared to Case 2, and completely mirror image results are observed for the mesenchymal cellular volume fraction. It signifies that the total volume of live cells decreases in Case 2 compared to Case 1. Because in Case 1, live cells need more oxygen to increase their population. Figure 11b indicates that the total tumor volume in Case 2 initially increases with time and then maintains an approximately linear growth profile. However, in Case 2, the tumor volume exhibits a sudden increase after the initial growth period. In Case 1, the tumor volume increases between the durations of $10 < t < 35$, after which it gradually decreases and attains linear growth. A key difference between the volume evolution of Case 1 and Case 2 is that the tumor in Case 2 achieves linear growth more quickly than the tumor in Case 1. Also, it is observed that the tumor in Case 1 exhibits sustained exponential growth compared to the tumor in Case 2 after the initial transition.

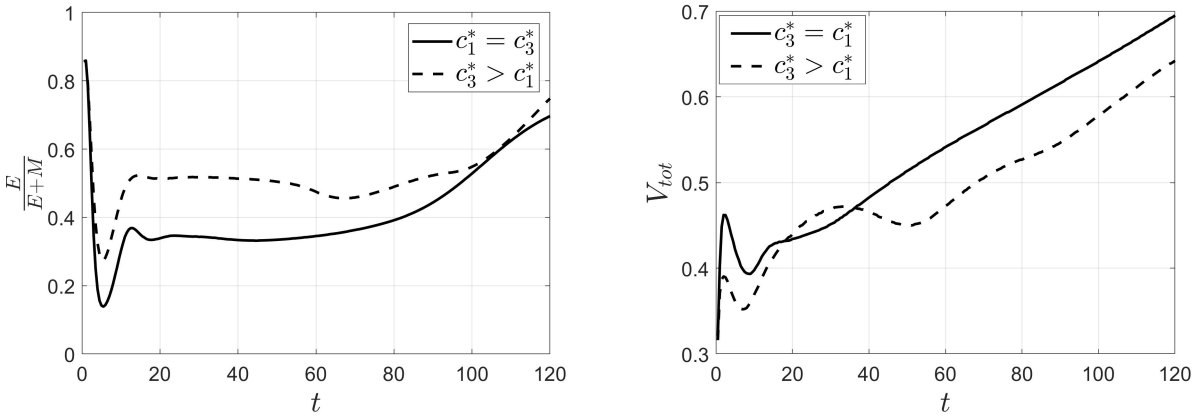

(a) (b)

Figure 11: The effects of the oxygen threshold value for the proliferation of epithelial and mesenchymal cells are examined (a) for epithelial cell volume fraction and (b) for total volume. Here, we consider for Case 1 $c_1^* = 0.6, c_3^* = 0.7$ and for Case 2 $c_1^* = c_3^* = 0.6$.

4.5. Influence of mesenchymal cells on EMT dynamics

Many studies report that mesenchymal cells can influence the transition from epithelial to mesenchymal and vice versa [53, 65]. In this section, we focus on how the mesenchymal population influences EMT and MET when the oxygen distribution is in a spatially heterogeneous environment. Recall from Eq (10) that the parameter δ represents the extent to which mesenchymal cells inhibit MET, and the parameter θ represents the strength with which mesenchymal cells promote EMT.

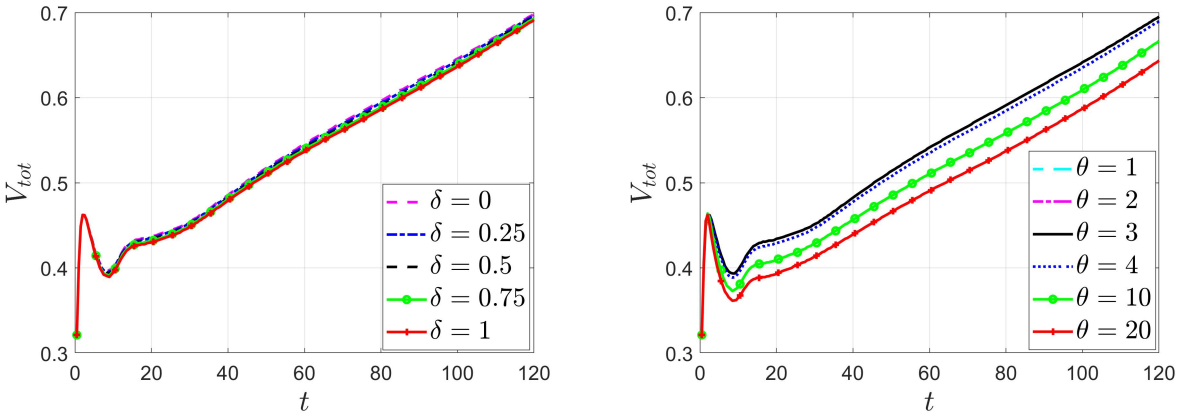

(a) (b)

Figure 12: *Effects of δ and θ on total volume of the tumor.*

We conducted a series of simulations varying δ and θ. The volume fraction of mesenchymal cells increases over time as the value of δ increases. This increase occurs because mesenchymal cells resist acquiring epithelial traits during the mesenchymal-epithelial transition (MET) process in a heterogeneous environment. Consequently, the volume fraction of epithelial cells decreases with higher values of δ. Changing δ does not affect the qualitative dynamics of the total tumor

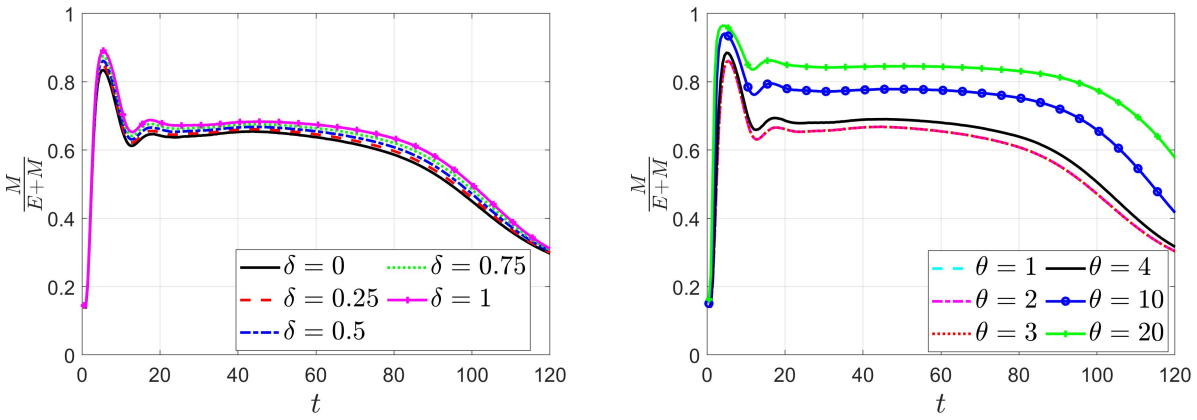

(a) (b)

Figure 13: *Effects of δ and θ on volume fraction of mesenchymal cells.*

volume. As expected, we observe a small decrease in the total tumor volume as δ increases (Figure 12a).

Varying the parameter θ has a more significant effect on the dynamics of mesenchymal cells than varying δ (Figure 13). This phenomenon occurs because mesenchymal cells influence epithelial cells to adopt mesenchymal characteristics, which also leads to a decrease in the fraction of epithelial cell volume. Epithelial cells proliferate rapidly, but their number decreases as θ increases, so that for a large value of θ we observe a decrease in total tumor volume (Figure 12b). In summary, we do not see any change in the tumor propagation speed or the dynamics of the total live volume fraction inside the tumor as θ and δ vary (results are not shown).

5. Discussion

In this study, we have investigated the effects of oxygen heterogeneity on epithelial to mesenchymal transitions (EMT) using the mathematical modeling framework. Our investigations primarily focus on (i) the effects of spatial oxygen heterogeneity on EMT dynamics, (ii) the impact of spatially homogeneous but fluctuation with time on EMT evolution, and (iii) the influence of mesenchymal cell diffusivity on EMT transition. The spatially homogeneous oxygen medium resembles the *in vitro* setup, while the heterogeneous oxygen environment represents the *in vivo* tumor. In addition, the function of the oxygen level with time in the growth medium is the practice of mimicking the *in vivo* event cyclic hypoxia. Moreover, we have examined how EMT dynamics is changed when the tumor is exposed to a high-level or low-level oxygen environment for a long time. Our proposed model is constructed based on partial differential equations (PDEs). The PDEs are derived using the principle of mass conservation to describe the time evolution of the epithelial, mesenchymal, and dead cell densities and oxygen concentration. Further, the proliferation of epithelial and mesenchymal cells, the transition from the epithelial to the mesenchymal phenotype (EMT), and the reverse process of the mesenchymal to epithelial transition (MET) are regulated by the local oxygen level at the tumor site. In the tumor, only mesenchymal cells have motile properties; this feature is captured in the model by incorporating random motility in the governing equation for mesenchymal cell density. Our proposed model is not the same as the analogy of the well-studied go-and-grow hypothesized mathematical models [32, 45], as both the population of

live cells in our model can proliferate.

We presented the numerical results, which show how the EMT dynamics is changed with oxygen levels. In laboratory-based experiments in a two-dimensional framework, the levels of nutrients and oxygen may be fixed or varied during the experiments, depending on the specific questions being addressed. As oxygen levels regulate EMT, MET, and the proliferation of epithelial and mesenchymal cells, the spatial homogeneous oxygen level in the tumor is examined to check its influence on the dynamics of EMT. For the oxygen level lower than the critical value of oxygen concentration for EMT induction, the tumor converts into mesenchymal type. For the oxygen level, which is higher than the oxygen threshold value for EMT initiation, the whole tumor eventually transformed into an epithelial type. These results indicate that a critical oxygen concentration in the tumor helps to switch from one phenotype to another phenotype. It is also experimentally observed [66]. In the *in vitro* context, the cyclic hypoxia phenomenon is mimicked by changing the oxygen environment in the culture medium on a periodic basis. Experimental studies suggest that the time interval of oxygen fluctuation may be short or long [62]. Hence, we have examined both the scenarios of long- and short-time periodicity of oxygen fluctuation on EMT induction. The simulation results for oxygen concentration are homogeneous in space and oscillate with time, showing a significant impact on EMT dynamics and tumor volume. Our prediction is that the shorter periodicity of the oxygen fluctuation in the growth environment leads to high tumor volume. We suggest that experiments be carried out to test this qualitative behaviour.

By performing numerical simulation, we investigated the impact of spatial oxygen heterogeneity on the EMT dynamics. We found that oxygen heterogeneity inside the tumor leads to phenotypic heterogeneity in the tumor. Also, it is observed that the population of epithelial cells at the initial time switches into mesenchymal phenotypic and, towards the end of the simulation, epithelial cells rapidly emerge at the outer portion of the tumor. Moreover, it is seen from the tumor-propagating velocity that the tumor initially grows exponentially, and thereafter the growth settles to approximately linear. It is a well-observed phenomenon in tumor biology [11]. Experimental works showed that mesenchymal cells could proliferate in harsh oxygen environments, whereas epithelial cells need an oxygen-nourished environment for mitotic cell division [44].

A series of numerical experiments are carried out to elucidate the impacts of mesenchymal cell diffusivity on EMT dynamics. We found that increasing the motility coefficient of the mesenchymal cells increases the propagation velocity of the tumor front point. However, epithelial cells are on the front seat of the tumor. It is observed that the motile property of mesenchymal cells helps to switch the mesenchymal population to the epithelial type in the heterogeneous spatial oxygen medium. In addition, we noticed that when the mesenchymal diffusivity is ignored after the initial transition periods, the densities of the mesenchymal and epithelial cells settle at a steady state. However, for non-zero diffusion coefficients for mesenchymal cells, the epithelial cell is the dominant population in the tumor in a quick time compared to the lower value of the motile coefficient. We further investigate the conditions under which invasion can be prevented. Our simulation results suggest that the tumor's invasive potential decreases as the MET rate increases. In addition, we observe that the tumor's invasive potential decreases as the oxygen consumption rates decrease. This behavior occurs because oxygen levels do not drop below the critical oxygen concentration for EMT when the oxygen consumption rate is small. As a result, all mesenchymal cells switch to the epithelial phenotype, which is not migratory. Hence, tumors are unable to increase their territory. We observed similar behavior in a spatially homogeneous oxygen field when the oxygen level in the growth medium exceeds the critical value for EMT.

There are many ways in which the proposed model in the article could be extended. The possible directions for future research include: the governing equation in this work may be easily extended into higher dimensions to study how the pattern changes during the EMT induction. In practice, tumors grow in 3-dimensions whereas, for simplicity, we formulate our model using a one-dimensional Cartesian geometry. We anticipate that recasting our model in a three-dimensional geometry would yield slightly different results, without altering their qualitative behaviour. In addition, *in vivo* tumors experience variability in their external environment. This phenomenon can be modeled by introducing a time-dependent oxygen supply at the tumor boundary [37]. This variation in oxygen leads to a phenotypically diverse tumor population [67, 68]. Investigating the impact of these oxygen variations on EMT dynamics would be an interesting avenue for future study. During the EMT process, epithelial cells do not convert into mesenchymal cells directly. Rather, an epithelial cell initially converts to a hybrid epithelial/mesenchymal state and then turns into the mesenchymal phenotype [69]. A similar protocol is followed when the reverse EMT, i.e., MET occurs. Therefore, the inclusion of a governing equation for the hybrid state in the proposed model would be a more detailed description of EMT dynamics. Besides oxygen heterogeneity in the tumor microenvironment, lactate, a byproduct of the anaerobic glucose metabolism process, also plays a role in initiating the EMT process [18, 35]. Hence, the interplay between lactate and EMT would give an interesting avenue for future research. Other directions that merit further consideration relate to validation and parameterization of the model against experimental data.

Acknowledgments

The first author of this article thanks the Ministry of Education, Govt. of India, for the research fellowship and the Indian Institute of Technology Guwahati, India, for the support provided during the period of this work.
This research was supported in part by the International Centre for Theoretical Sciences (ICTS) for the program - Theoretical approaches in cancer progression and treatment (code: ICTS/MATHONCO 2024/03).

Ethical approval: The authors did not conduct any research with humans or animals.
Conflict of interest: On behalf of all authors, the corresponding author states that there is no conflict of interest.

References

[1] Shubham Tripathi, Herbert Levine, and Mohit Kumar Jolly. The physics of cellular decision making during epithelial–mesenchymal transition. Annual Review of Biophysics, 49(1):1–18, 2020.

[2] Alisha M Mendonsa, Tae-Young Na, and Barry M Gumbiner. E-cadherin in contact inhibition and cancer. Oncogene, 37(35):4769–4780, 2018.

[3] Lorenz Isert, Aditi Mehta, Gabriele Loiudice, Altea Oliva, Andreas Roidl, and Olivia M Merkel. An in vitro approach to model emt in breast cancer. International Journal of Molecular Sciences, 24(9):7757, 2023.

[4] Jacqueline Banyard and Diane R Bielenberg. The role of emt and met in cancer dissemination. Connective Tissue Research, 56(5):403–413, 2015.

[5] Amparo Cano, Mirna A Pérez-Moreno, Isabel Rodrigo, Annamaria Locascio, María J Blanco, Marta G del Barrio, Francisco Portillo, and M Angela Nieto. The transcription factor snail controls epithelial–mesenchymal transitions by repressing e-cadherin expression. Nature Cell Biology, 2(2):76–83, 2000.

[6] Gema Moreno-Bueno, F Portillo, and Amparo Cano. Transcriptional regulation of cell polarity in emt and cancer. Oncogene, 27(55):6958–6969, 2008.

[7] Hassan Fazilaty, Luciano Rago, Khalil Kass Youssef, Oscar H Ocaña, Francisco Garcia-Asencio, Aida Arcas, Juan Galceran, and M Angela Nieto. A gene regulatory network to control emt programs in development and disease. Nature Communications, 10(1):5115, 2019.

[8] Sudipa Saha Roy, Vijaya Kumar Gonugunta, Abhik Bandyopadhyay, Manjeet K Rao, Gregory J Goodall, LuZhe Sun, Rajeshwar R Tekmal, and Ratna K Vadlamudi. Significance of pelp1/hdac2/mir-200 regulatory network in emt and metastasis of breast cancer. Oncogene, 33(28):3707–3716, 2014.

[9] Ewa Nowak and Ilona Bednarek. Aspects of the epigenetic regulation of emt related to cancer metastasis. Cells, 10(12):3435, 2021.

[10] Elad Katz, Sylvie Dubois-Marshall, Andrew H Sims, Philippe Gautier, Helen Caldwell, Richard R Meehan, and David J Harrison. An in vitro model that recapitulates the epithelial to mesenchymal transition (emt) in human breast cancer. PloS One, 6(2):e17083, 2011.

[11] Douglas Hanahan and Robert A Weinberg. The hallmarks of cancer. Cell, 100(1):57–70, 2000. doi:10.1016/S0092-8674(00)81683-9.

[12] Brooke A Brown, Paul J Myers, Sara J Adair, Jason R Pitarresi, Shiv K Sah-Teli, Logan A Campbell, William S Hart, Michelle C Barbeau, Kelsey Leong, Nicholas Seyler, et al. A histone methylation–mapk signaling axis drives durable epithelial–mesenchymal transition in hypoxic pancreatic cancer. Cancer Research, 84(11):1764–1780, 2024.

[13] Kristine Yttersian Sletta, Maria K Tveitarås, Ning Lu, Agnete ST Engelsen, Rolf K Reed, Annette Garmann-Johnsen, and Linda Stuhr. Oxygen-dependent regulation of tumor growth and metastasis in human breast cancer xenografts. PloS One, 12(8):e0183254, 2017.

[14] Shing Yau Tam, Vincent WC Wu, and Helen KW Law. Hypoxia-induced epithelial-mesenchymal transition in cancers: Hif-1α and beyond. Frontiers in Oncology, 10:486, 2020.

[15] Lin Zhang, Gang Huang, Xiaowu Li, Yujun Zhang, Yan Jiang, Junjie Shen, Jia Liu, Qingliang Wang, Jin Zhu, Xiaobin Feng, et al. Hypoxia induces epithelial-mesenchymal transition via activation of snai1 by hypoxia-inducible factor-1α in hepatocellular carcinoma. BMC Cancer, 13:1–9, 2013.

[16] Haseeb Zubair, Shafquat Azim, Sanjeev Kumar Srivastava, Aamir Ahmad, Arun Bhardwaj, Mohammad Aslam Khan, Girijesh Kumar Patel, Sumit Arora, James Elliot Carter, Seema Singh, et al. Glucose metabolism reprogrammed by overexpression of ikk promotes pancreatic tumor growth. Cancer Research, 76(24):7254–7264, 2016. doi:10.1158/0008-5472.CAN-16-1666.

[17] Maymona Al-Husari and Steven D. Webb. Regulation of tumour intracellular ph: A mathematical model examining the interplay between h+ and lactate. Journal of Theoretical Biology, 322:58–71, 2013. doi:10.1016/j.jtbi.2013.01.007.

[18] Xiangrui Li, Zhijian Zhang, Yao Zhang, Yuxiang Cao, Huijun Wei, and Zhihao Wu. Upregulation of lactate-inducible snail protein suppresses oncogene-mediated senescence through p16 ink4a inactivation. Journal of Experimental & Clinical Cancer Research, 37:1–13, 2018.

[19] Joshua Adam Bull and Helen Mary Byrne. The hallmarks of mathematical oncology. Proceedings of the IEEE, 110(5):523–540, 2022.

[20] Philip J Murray, Carina M Edwards, Marcus J Tindall, and Philip K Maini. From a discrete to a continuum model of cell dynamics in one dimension. Physical Review E—Statistical, Nonlinear, and Soft Matter Physics, 80(3):031912, 2009.

[21] Adam L MacLean, Heather A Harrington, Michael PH Stumpf, and Marc DH Hansen. Epithelial-mesenchymal transition in metastatic cancer cell populations affects tumor dormancy in a simple mathematical model. Biomedicines, 2(4):384–402, 2014.

[22] Chiara Simeoni, Simona Dinicola, Alessandra Cucina, Corrado Mascia, and Mariano Bizzarri. Systems biology approach and mathematical modeling for analyzing phase-space switch during epithelial-mesenchymal transition. Systems Biology, pages 95–123, 2018.

[23] Andrew Dhawan, Seyed Ali Madani Tonekaboni, Joseph H Taube, Stephen Hu, Nathalie Sphyris, Sendurai A Mani, and Mohammad Kohandel. Mathematical modelling of phenotypic plasticity and conversion to a stem-cell state under hypoxia. Scientific Reports, 6(1): 18074, 2016.

[24] Peng He, Kang Qiu, and Ya Jia. Modeling of mesenchymal hybrid epithelial state and phenotypic transitions in emt and met processes of cancer cells. Scientific Reports, 8(1):14323, 2018.

[25] Shubham Tripathi, Priyanka Chakraborty, Herbert Levine, and Mohit Kumar Jolly. A mechanism for epithelial-mesenchymal heterogeneity in a population of cancer cells. PLoS Computational Biology, 16(2):e1007619, 2020.

[26] Gopinath Sadhu and DC Dalal. Effects of non-linear interaction between oxygen and lactate on solid tumor growth under cyclic hypoxia. Bulletin of Mathematical Biology, 87(3):41, 2025.

[27] KS Yadav and Gopinath Sadhu. Effect of inosine on recurrence of tumor after radiation therapy: A mathematical investigation. Journal of Theoretical Biology, page 112138, 2025.

[28] Helen M Byrne, John R King, DL Sean McElwain, and Luigi Preziosi. A two-phase model of solid tumour growth. Applied Mathematics Letters, 16(4):567–573, 2003. doi:10.1016/S0893-9659(03)00038-7.

[29] Rebecca M Crossley, Kevin J Painter, Tommaso Lorenzi, Philip K Maini, and Ruth E Baker. Phenotypic switching mechanisms determine the structure of cell migration into extracellular matrix under the 'go-or-grow'hypothesis. Mathematical Biosciences, page 109240, 2024.

[30] Linnea C Franssen and Mark AJ Chaplain. A mathematical multi-organ model for bidirectional epithelial–mesenchymal transitions in the metastatic spread of cancer. IMA Journal of Applied Mathematics, 85(5):724–761, 2020.

[31] Mark AJ Chaplain and G Lolas. Mathematical modelling of cancer invasion of tissue: dynamic heterogeneity. Networks and Heterogeneous Media, 1(3):399–439, 2006. doi:10.3934/nhm.2006.1.399.

[32] Haralampos Hatzikirou, David Basanta, Matthias Simon, K Schaller, and Andreas Deutsch. 'go or grow': the key to the emergence of invasion in tumour progression? Mathematical Medicine and Biology: a Journal of the IMA, 29(1):49–65, 2012.

[33] C Venkata Sai Prasanna, Mohit Kumar Jolly, and Ramray Bhat. Spatial heterogeneity in tumor adhesion qualifies collective cell invasion. Biophysical Journal, 2024.

[34] Yingying Jing, Zhipeng Han, Shanshan Zhang, Yan Liu, and Lixin Wei. Epithelial-mesenchymal transition in tumor microenvironment. Cell & bioscience, 1(1):29, 2011.

[35] Dongya Jia, Jun Hyoung Park, Harsimran Kaur, Kwang Hwa Jung, Sukjin Yang, Shubham Tripathi, Madeline Galbraith, Youyuan Deng, Mohit Kumar Jolly, Benny Abraham Kaipparettu, et al. Towards decoding the coupled decision-making of metabolism and epithelial-to-mesenchymal transition in cancer. British Journal of Cancer, 124(12):1902–1911, 2021.

[36] Nikolaos Sfakianakis, Niklas Kolbe, Nadja Hellmann, and Mária Lukáčová-Medvid'ová. A multiscale approach to the migration of cancer stem cells: Mathematical modelling and simulations. Bulletin of mathematical biology, 79(1):209–235, 2017.

[37] Ryan J Murphy, Gency Gunasingh, Nikolas K Haass, and Matthew J Simpson. Growth and adaptation mechanisms of tumour spheroids with time-dependent oxygen availability. PLOS Computational Biology, 19(1):e1010833, 2023.

[38] Milad Shamsi, Mohsen Saghafian, Morteza Dejam, and Amir Sanati-Nezhad. Mathematical modeling of the function of warburg effect in tumor microenvironment. Scientific reports, 8 (1):8903, 2018.

[39] Thomas D Lewin, Philip K Maini, Eduardo G Moros, Heiko Enderling, and Helen M Byrne. A three phase model to investigate the effects of dead material on the growth of avascular tumours. Mathematical Modelling of Natural Phenomena, 15:22, 2020. doi:10.1051/mmnp/2019039.

[40] HP Greenspan. Models for the growth of a solid tumor by diffusion. Studies in Applied Mathematics, 51(4):317–340, 1972. doi:10.1002/sapm1972514317.

[41] Joseph J Casciari, Stratis V Sotirchos, and Robert M Sutherland. Mathematical modelling of microenvironment and growth in emt6/ro multicellular tumour spheroids. Cell Proliferation, 25(1):1–22, 1992. doi:10.1111/j.1365-2184.1992.tb01433.x.

[42] Markus R Owen, Tomás Alarcón, Philip K Maini, and Helen M Byrne. Angiogenesis and vascular remodelling in normal and cancerous tissues. Journal of mathematical biology, 58 (4):689–721, 2009.

[43] Thomas D Lewin, Helen M Byrne, Philip K Maini, Jimmy J Caudell, Eduardo G Moros, and Heiko Enderling. The importance of dead material within a tumour on the dynamics in response to radiotherapy. Physics in Medicine & Biology, 65(1):015007, 2020.

[44] Shuo Chen, Xi Chen, Wei Li, Tao Shan, Wan Run Lin, Jiancang Ma, Xijuan Cui, Wenbin Yang, Gang Cao, Yiming Li, et al. Conversion of epithelial-to-mesenchymal transition to mesenchymal-to-epithelial transition is mediated by oxygen concentration in pancreatic cancer cells. Oncology letters, 15(5):7144–7152, 2018.

[45] Tracy L Stepien, Erica M Rutter, and Yang Kuang. Traveling waves of a go-or-grow model of glioma growth. SIAM Journal on Applied Mathematics, 78(3):1778–1801, 2018.

[46] Youyuan Deng, Herbert Levine, Xiaoming Mao, and Leonard M Sander. Collective motility and mechanical waves in cell clusters. The European Physical Journal E, 44(11):137, 2021.

[47] Eric Theveneau and Roberto Mayor. Collective cell migration of epithelial and mesenchymal cells. Cellular and Molecular Life Sciences, 70(19):3481–3492, 2013.

[48] David Robert Grimes, Catherine Kelly, Katarzyna Bloch, and Mike Partridge. A method for estimating the oxygen consumption rate in multicellular tumour spheroids. Journal of The Royal Society Interface, 11(92):20131124, 2014. doi:10.1098/rsif.2013.1124.

[49] Kristin R Swanson, Ellsworth C Alvord Jr, and James D Murray. A quantitative model for differential motility of gliomas in grey and white matter. Cell Proliferation, 33(5):317–329, 2000. doi:10.1046/j.1365-2184.2000.00177.x.

[50] CJW Breward, HM Byrne, and CE Lewis. Modelling the interactions between tumour cells and a blood vessel in a microenvironment within a vascular tumour. European Journal of Applied Mathematics, 12(5):529–556, 2001. doi:10.1017/S095679250100448X.

[51] Adam L MacLean, Heather A Harrington, Michael PH Stumpf, and Marc DH Hansen. Epithelial-mesenchymal transition in metastatic cancer cell populations affects tumor dormancy in a simple mathematical model. Biomedicines, 2(4):384–402, 2014. doi:10.3390/biomedicines2040384.

[52] Kazuhiro Suzuki, Ruowen Sun, Makoto Origuchi, Masahiko Kanehira, Takenori Takahata, Jugoh Itoh, Akihiro Umezawa, Hiroshi Kijima, Shinsaku Fukuda, and Yasuo Saijo. Mesenchymal stromal cells promote tumor growth through the enhancement of neovascularization. Molecular Medicine, 17:579–587, 2011. doi:10.2119/molmed.2010.00157.

[53] Paras Jain, Ramanarayanan Kizhuttil, Madhav B Nair, Sugandha Bhatia, Erik W Thompson, Jason T George, and Mohit Kumar Jolly. Cell-state transitions and frequency-dependent interactions among subpopulations together explain the dynamics of spontaneous epithelial-mesenchymal heterogeneity in breast cancer. bioRxiv, pages 2023–12, 2023. doi:10.1101/2023.12.07.567986.

[54] Mizuki Yamamoto, Kota Sakane, Kana Tominaga, Noriko Gotoh, Takayoshi Niwa, Yasuko Kikuchi, Keiichiro Tada, Naoki Goshima, Kentaro Semba, and Jun-ichiro Inoue. Intratumoral bidirectional transitions between epithelial and mesenchymal cells in triple-negative breast cancer. Cancer Science, 108(6):1210–1222, 2017. doi:10.1111/cas.13246.

[55] Sugandha Bhatia, James Monkman, Tony Blick, Cletus Pinto, Mark Waltham, Shivashankar H Nagaraj, and Erik W Thompson. Interrogation of phenotypic plasticity between epithelial and mesenchymal states in breast cancer. Journal of Clinical Medicine, 8(6):893, 2019. doi:10.3390/jcm8060893.

[56] Tanvi V Joshi, Daniele Avitabile, and Markus R Owen. Capturing the dynamics of a hybrid multiscale cancer model with a continuum model. Bulletin of Mathematical Biology, 80(6): 1435–1475, 2018.

[57] Antonina Lavrentieva, Ingrida Majore, Cornelia Kasper, and Ralf Hass. Effects of hypoxic culture conditions on umbilical cord-derived human mesenchymal stem cells. Cell Communication and Signaling, 8:1–9, 2010.

[58] Michael L Felder, Aaron D Simmons, Robert L Shambaugh, and Vassilios I Sikavitsas. Effects of flow rate on mesenchymal stem cell oxygen consumption rates in 3d bone-tissue-engineered constructs cultured in perfusion bioreactor systems. Fluids, 5(1):30, 2020.

[59] EABF Lima, N Ghousifam, A Ozkan, JT Oden, A Shahmoradi, MN Rylander, B Wohlmuth, and TE Yankeelov. Calibration of multi-parameter models of avascular tumor growth using time resolved microscopy data. Scientific Reports, 8(1):14558, 2018. doi:10.1038/s41598-018-32347-9.

[60] John David Anderson, Gérard Degrez, Erik Dick, and Roger Grundmann. Computational fluid dynamics: an introduction. Springer Science & Business Media, 2013.

[61] Samuel B Bader, Mark W Dewhirst, and Ester M Hammond. Cyclic hypoxia: an update on its characteristics, methods to measure it and biological implications in cancer. Cancers, 13 (1):23, 2020.

[62] Carine Michiels, Céline Tellier, and Olivier Feron. Cycling hypoxia: A key feature of the tumor microenvironment. Biochimica et Biophysica Acta (BBA)-Reviews on Cancer, 1866 (1):76–86, 2016.

[63] Peter W Vaupel, Stanley Frinak, and Haim I Bicher. Heterogeneous oxygen partial pressure and ph distribution in c3h mouse mammary adenocarcinoma. Cancer Research, 41(5):2008–2013, 1981.

[64] Sarah M Ridge, Francis J Sullivan, and Sharon A Glynn. Mesenchymal stem cells: key players in cancer progression. Molecular cancer, 16(1):31, 2017.

[65] Ievgenia Pastushenko, Audrey Brisebarre, Alejandro Sifrim, Marco Fioramonti, Tatiana Revenco, Soufiane Boumahdi, Alexandra Van Keymeulen, Daniel Brown, Virginie Moers, Sophie Lemaire, et al. Identification of the tumour transition states occurring during emt. Nature, 556(7702):463–468, 2018.

[66] Rob A Cairns, Tuula Kalliomaki, and Richard P Hill. Acute (cyclic) hypoxia enhances spontaneous metastasis of kht murine tumors. Cancer research, 61(24):8903–8908, 2001.

[67] Aleksandra Ardaševa, Robert A Gatenby, Alexander RA Anderson, Helen M Byrne, Philip K Maini, and Tommaso Lorenzi. A mathematical dissection of the adaptation of cell populations to fluctuating oxygen levels. Bulletin of Mathematical Biology, 82(6):81, 2020.

[68] Aleksandra Ardaševa, Robert A Gatenby, Alexander RA Anderson, Helen M Byrne, Philip K Maini, and Tommaso Lorenzi. Evolutionary dynamics of competing phenotype-structured populations in periodically fluctuating environments. Journal of mathematical biology, 80 (3):775–807, 2020.

[69] Mohit Kumar Jolly, Marcelo Boareto, Bin Huang, Dongya Jia, Mingyang Lu, Eshel Ben-Jacob, José N Onuchic, and Herbert Levine. Implications of the hybrid epithelial/mesenchymal phenotype in metastasis. Frontiers in oncology, 5:155, 2015.